





Article

Effect of Modified Alumina Support on the Performance of Ni-Based Catalysts for CO₂ Reforming of Methane

Salwa Bader Alreshaidan ^{1,*}, Ahmed A. Ibrahim ^{2,*}, Anis H. Fakeeha ² , Abdulaziz M. Almutlaq ² ,
Fekri Abdurqab Ahmed Ali ²  and Ahmed S. Al-Fatesh ^{2,*} 

¹ Department of Chemistry, Faculty of Science, King Saud University, P.O. Box 800, Riyadh 11451, Saudi Arabia

² Chemical Engineering Department, College of Engineering, King Saud University, P.O. Box 800, Riyadh 11421, Saudi Arabia

* Correspondence: chem241@ksu.edu.sa (S.B.A.); aidid@ksu.edu.sa (A.A.I.); aalfatesh@ksu.edu.sa (A.S.A.-F.); Tel.: +966-505207824 (S.B.A.); +966-534278905 (A.A.I.); +966-11-467-6859 (A.S.A.-F.)

Abstract: The CO₂ reforming of methane to syngas was examined over five different supported catalysts. In this study, 5% Ni was used as the active metal part of the catalyst. To better comprehend the impact of the supports on the catalytic properties, 5% Ni-based catalysts were characterized using nitrogen adsorption–desorption isotherms, XRD, H₂-TPR, CO₂-TPD, TGA, TPO, FTIR, and Raman. The results showed that the catalyst support with the highest surface area provided the best catalytic activity. The acquired CH₄ and CO₂ conversions at 700 °C were 58.2% and 67.6%, respectively, with a hydrogen/carbon ratio of 0.85. The TGA investigation of the high-surface-area sample produced a minimum carbon deposition of 11.2 wt.%, and in the CO₂-TPD investigation, the high-surface-area sample exhibited the absence of a peak in the strong-basic-sites zone. The formation of NiAl₂O₄ spinel, moderate basicity, and the high surface area explained the outperformance of the high-surface-area catalyst sample.

Keywords: alumina; CO₂ reforming of methane; support; nickel catalyst; silica



Citation: Alreshaidan, S.B.; Ibrahim, A.A.; Fakeeha, A.H.; Almutlaq, A.M.; Ali, F.A.A.; Al-Fatesh, A.S. Effect of Modified Alumina Support on the Performance of Ni-Based Catalysts for CO₂ Reforming of Methane. *Catalysts* **2022**, *12*, 1066. <https://doi.org/10.3390/catal12091066>

Academic Editors: Maria A. Goula and Antonio Vita

Received: 18 August 2022

Accepted: 13 September 2022

Published: 18 September 2022

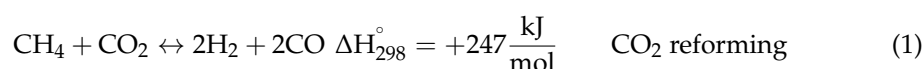
Publisher's Note: MDPI stays neutral with regard to jurisdictional claims in published maps and institutional affiliations.

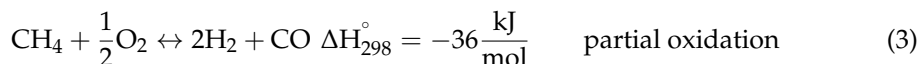
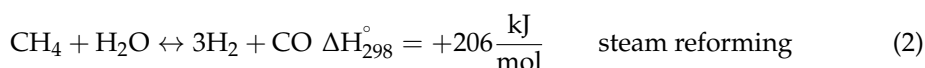


Copyright: © 2022 by the authors. Licensee MDPI, Basel, Switzerland. This article is an open access article distributed under the terms and conditions of the Creative Commons Attribution (CC BY) license (<https://creativecommons.org/licenses/by/4.0/>).

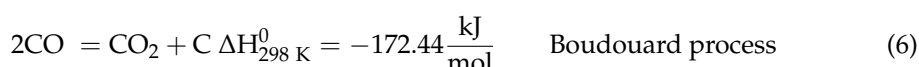
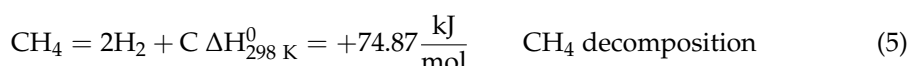
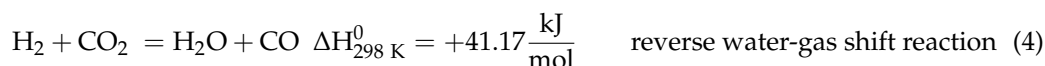
1. Introduction

Heterogeneous catalysis is a vital part of energy and sustainability research because it permits chemical transformations to be performed at somewhat low temperatures while decreasing or circumventing the formation of by-products [1–3]. Up to now, heterogeneous catalysts based on transition metals have been found to be successful in the hydrogenation of petroleum refining and processing, as well as in the manufacture of fine and bulk chemicals [4]. Catalytic hydrogenation primarily uses precious metals such as Pd and Pt, which are characterized by high prices and rarity. Thus, research has turned to nonprecious metals to identify lower-cost and more widely available hydrogenation catalysts [5–7]. Transition metals such as Fe, Co, and Ni have received great attention because of their specific qualities: huge abundance, low cost, lack of toxicity, and distinctive catalytic properties [8]. CO₂ reforming of methane (CRM), adopted in this study, is a process that transforms CH₄ and CO₂ greenhouse gases (GHGs) into synthesis gas ('syngas', a mixture of CO and H₂) [9–12]. Today, CH₄ and CO₂ emissions to the atmosphere are increasing our concern for the environment. However, this process promotes sustainable energy as methane is the principal element in natural gas (>85%) [13]. The use of GHGs during the reforming processes leads to their conversion to hydrogen, which is an indispensable material for all petrochemical industries and renewable energy sources, whilst also mitigating the environmental impact of GHGs emitted to the atmosphere. The well-studied processes for reforming methane are through steam, partial oxidation, and dry or CO₂ [1,2]. Their primary reforming reactions for the generation of syngas are:





CRM generates syngas with an equal H₂/CO ratio, which is suitable for F-T synthesis to give liquid fuel [2]. However, this process presents challenges—chiefly, high endothermicity and carbon deposition—restricting the commercial practice of CRM [3]. The targeted Equation (1) is also accompanied by side reactions:



Ni-based catalysts are the most active for low-temperature CRM. SiO₂ and Al₂O₃ are two typical catalyst supports for CRM because of their high thermal stability and surface area. The alumina support has been well commercialized for its hardness, chemical and wear resistance, and wide raw material availability [4]. Nickel-based catalysts undergo deactivation owing to carbon formation and sintering of metallic particles because of their lack of thermal stability [5,6]. A catalyst support plays a vital role as it can assist in stabilizing the metallic particles via efficient interactions with the supporting metallic particles, diminishing the coke formation and the sintering of the metallic particles [7–9]. In this way, to avoid small Ni clusters on Al₂O₃ supports forming larger Ni particles at high temperatures, the strong metal–support interaction between Ni and Al₂O₃ is considered to upgrade the thermal stability of small Ni particles, which helps the formation of spinel NiAl₂O₄ [10,11]. By doing so, carbon deposition can be tackled from the viewpoint of the catalyst structure. Together with the nature of the support, its morphology has additionally been revealed to be able to modify the size and dispersion of the supported metallic particles, enhancing their catalytic performance by low coke formation and metal sintering [9,12]. Wang et al. [13] also demonstrated that the metal–support interaction plays an important role in controlling the catalyst sintering and carbon deposition. In the study, the deposition of carbonaceous species was controlled as a result of the Ni–support interaction [13]. Thus, the spread of Ni on the surface of the catalyst and the structure of the support appear the prime means of resolving the deactivation problem. Elharati et al. investigated the effect of a silica oxide support on the catalytic activity of a nickel-molybdenum catalyst for hydrogen production and found that the SiO₂ morphology improved the coking resistance of Ni [14]. Xu et al. reported the results of 10% Ni supported on either silica or alumina used for CRM [15]. The result displayed that the performance was affected by the type of support. For instance, a silica-support catalyst exhibited higher initial activity but poor stability when operated at 800 °C, whereas the alumina-supported catalyst provided lower activity but much higher stability. Zhang et al. studied low-temperature CRM using Ni supported on either SiO₂ or γ-Al₂O₃ [16]. Their results showed excessive CH₄ decomposition when using the silica support, leading to poor activity and stability. With respect to Ni/γ-Al₂O₃, a good metal–support interaction was developed, facilitating a stable performance, which preferentially accelerated CO₂ adsorption and dissociation.

Promoting the CO₂ gasification of coke is a vital step for coke reduction on the surface of the catalysts [17]. Alkaline metals have been tested as promoters to enhance coke resistivity of Ni-based catalysts by helping the adsorption and activation of CO₂ during CRM. Cao et al. investigated the stabilization of CRM on modified Ni/Al₂O₃ catalysts via an in situ K₂CO₃-enabled dynamic coke elimination reaction. It was discovered that the doping of potassium carbonate enhanced the coke resistance [18]. Garbarino et al. examined the effect of mixed supports of alumina and silica for Ni-based catalysts and found that

silica in fair amounts considerably modified the dispersing properties of alumina [19]. Silica doping was discovered to increase thermal stability and improve the porosity of alumina supports, whilst additionally increasing the reducibility of alumina-supported metal catalysts [20]. This study the influence of alumina and modified alumina supports on Ni-based catalysts operated for CO₂ reforming of methane for synthesis gas. The impacts of the high-hydrothermal-stability supports for CO₂ reforming are compared and summarized in terms of greenhouse gas conversions. The Ni-supported catalysts were prepared by the impregnation method and their catalytic performances were tested in a CRM reaction. The catalytic performance of the catalysts in CRM was explained using the BET, XRD, TPR, TPD, TPR, FTIR, Raman, TGA, and TPO characterization methods.

2. Results and Discussion

2.1. BET Analysis

The textural properties of the fresh catalysts were investigated by N₂ adsorption–desorption measurements, as shown in Figure 1. The isotherms in Figure 1 are of type IV with H₃ hysteresis loops according to IUPAC sorting. These trends are characteristic of mesoporous materials and are usually found on solids consisting of masses of particles forming slit-shaped pores of various sizes and shapes [21]. Nevertheless, it can be observed from Figure 1 that nitrogen uptake began at a relative pressure range of 0.6–0.7. The highest-surface-area sample (SA75) adsorbed the greatest quantity of N₂ (400 cm³/g), while SA02, with a low surface area, adsorbed the lowest quantity of N₂ (0.4 cm³/g).

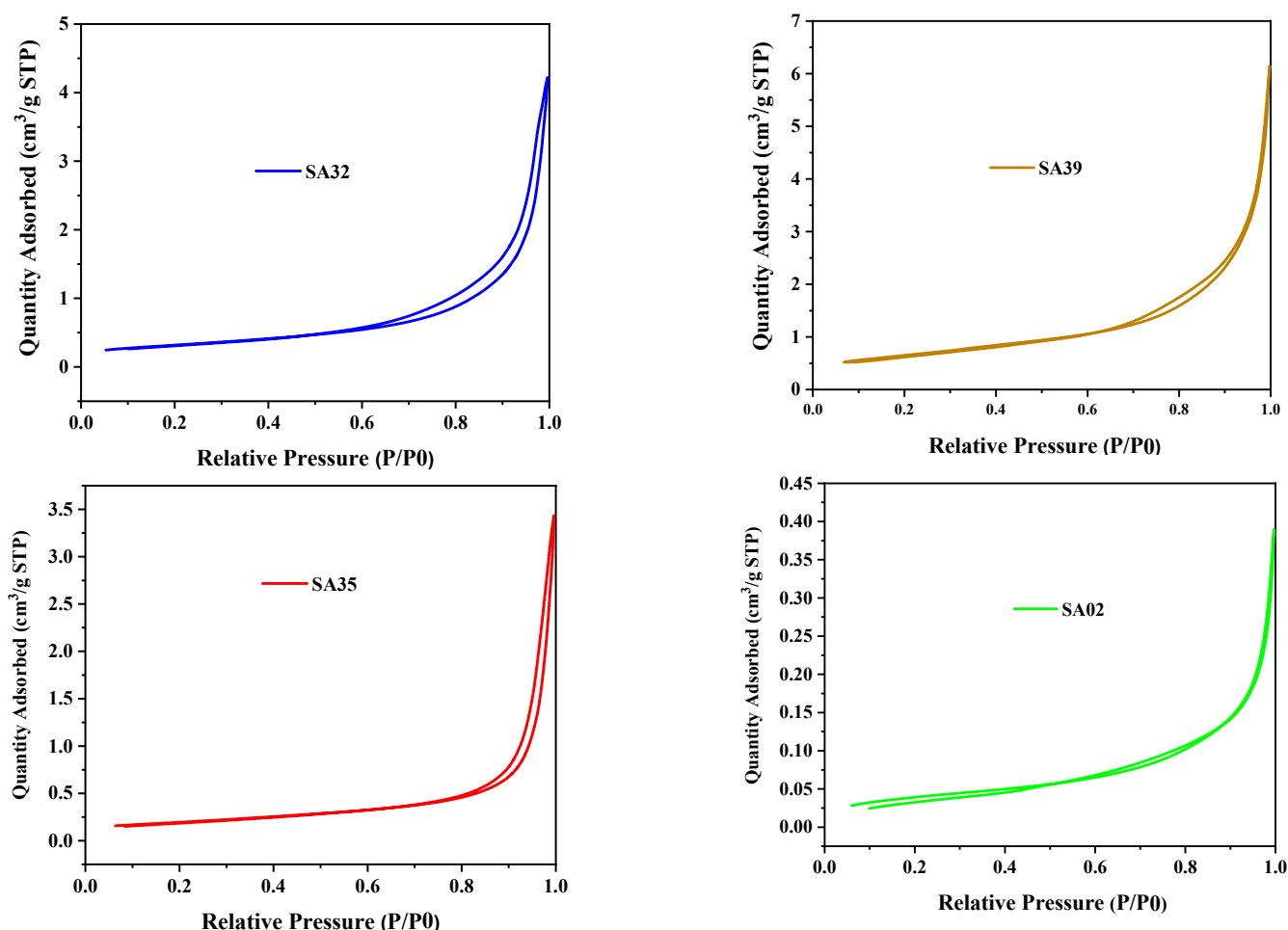


Figure 1. Cont.

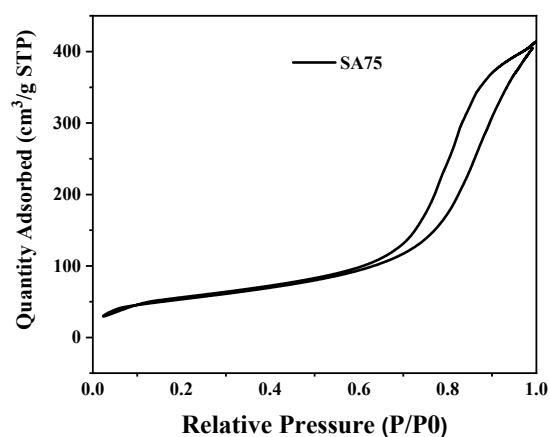


Figure 1. N₂ adsorption–desorption measurements of fresh Ni-supported catalysts.

2.2. TPR

H₂-TPR (temperature-programmed reduction) curves of the fresh catalysts are shown in Figure 2. In the range of 0–330 °C, peaks did not appear, indicating that there was no free NiO in the samples. Practically, all the samples were characterized by a single broad peak. The peaks for SA39 at 368 °C, SA35 at 460 °C, and SA02 at 470 °C could be attributed to moderate interactions between NiO and the support. Comparatively, the peak for SA32 at 671 °C could be ascribed to the strong interaction between NiO and the support. Meanwhile, the peak at 825 °C for SA75 could be related to the formation of NiAl₂O₄, which was caused by the strong interaction of Al₂O₃ with NiO [22].

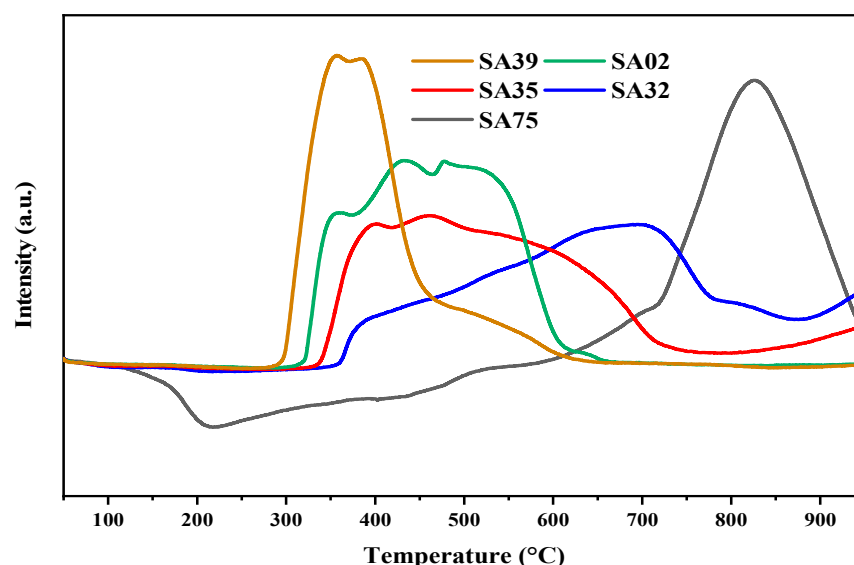


Figure 2. H₂-TPR profiles of fresh Ni-supported catalysts.

2.3. XRD Analysis

To identify the phases, Figure 3 shows the XRD profiles of fresh catalysts. XRD peaks of Al₂O₃ and NiAl₂O₄ appear in Figure 3 at $2\theta = 37.3, 46.0,$ and 66.5° (JCPDS 86-1410). The peaks for NiO overlay those of Al₂O₃ and appear at $2\theta = 37.3, 46.0,$ and 66.5° (JCPDS 47-1049), with the reflections of 111, 200, and 220, respectively, indicating that these Ni-comprising phases were highly scattered on the surface of the supports [23]. Commonly, a broad peak at around 22° was found for the Ni/SiO₂ catalysts, which were assigned to silica.

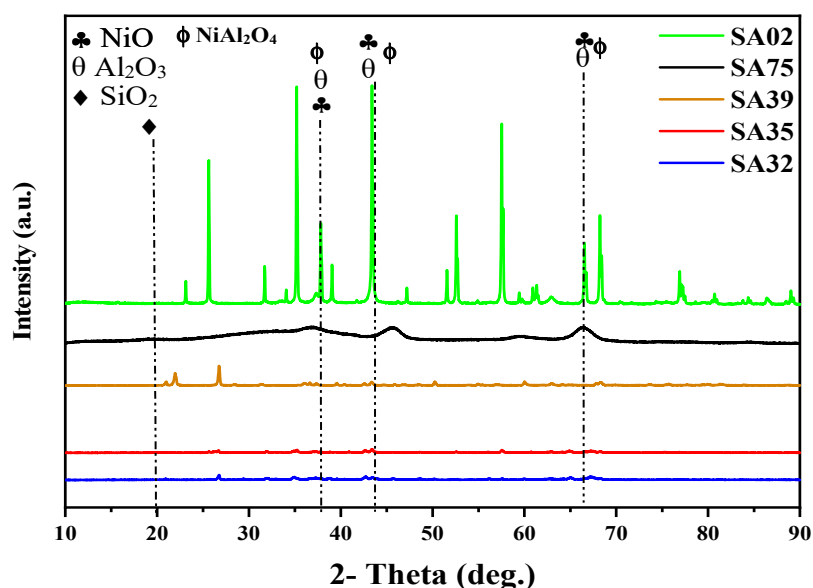


Figure 3. XRD patterns of fresh Ni-supported catalysts.

2.4. FTIR Analysis

Figure 4 displays the Fourier transform infrared spectra of the different Ni-supported catalysts. A wide band extending from 550 to 840 cm^{-1} can be ascribed to the Al-O stretching vibrations of the tetrahedron (AlO_4) and octahedron (AlO_6) environments [24]. The IR spectrum of samples also shows bands at 1640 cm^{-1} and 3450 cm^{-1} for stretching and bending vibration of O-H, respectively [25]. Apart from that IR band, for unidentate carbonate at 1384 cm^{-1} and for stretching of C-H (in format species) at 2850 cm^{-1} , a combination of asymmetric stretching of COO and bending vibration of the C-H bond at 2925 cm^{-1} can additionally be observed [26]. The IR spectra show broad transmission bands centered at 550 and 612 cm^{-1} typical for Ni-O stretching vibrations [27].

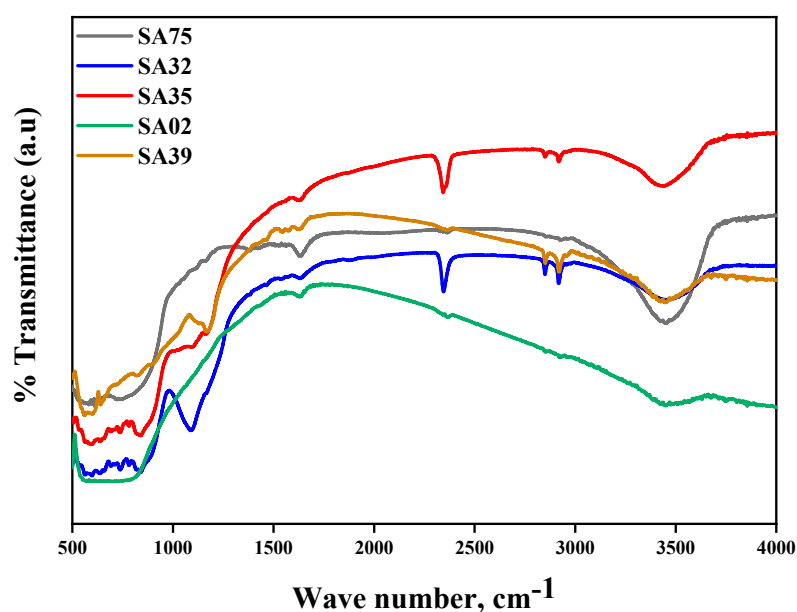


Figure 4. Evolution of the IR spectra of the Ni-supported samples.

2.5. CO_2 -TPD

The surface concentrations of the basic sites were determined by temperature-programmed desorption of carbon dioxide (CO_2 -TPD). Figure 5 shows the CO_2 -TPD measurements performed in the temperature range of 50–800 $^\circ\text{C}$ at a rate of 10 $^\circ\text{C}/\text{min}$ using

helium (25 STP ml/min) as the carrier flow. The catalysts displayed peaks in the three zones of the basicity: weak, medium, and strong, at temperatures of 0–200 °C, 200–350 °C, and 350–600 °C, respectively. The weak basicity is attributed to surface hydroxyl resulting from physical adsorption; the medium-strength basic sites are assigned to surface oxygen anions resulting from the chemical adsorption; the strong basic sites are attributed to the bulk oxygen anion/oxygen vacancy resulting from the interaction with oxygen vacancies. SA39, SA02, and SA35 possess basic sites in all three zones, with the highest intensities in the strong zone. The excessive basicity in this system stimulated a high extent of CO₂ dissociation (CO₂ = C + O₂) to occur and, therefore, deactivated the catalyst, as reflected by the TGA analysis. The SA75 sample with the highest activity and stability did not produce a peak in the strong-basic-sites zone.

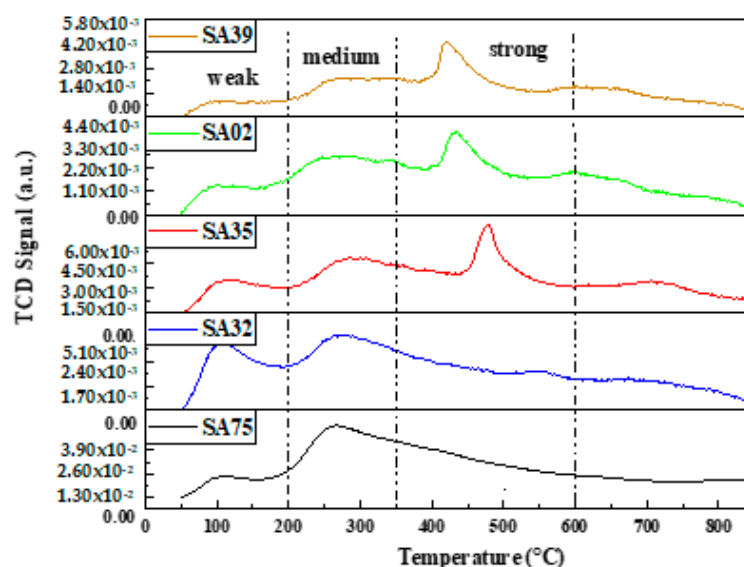


Figure 5. Fresh CO₂-TPD analysis of Ni-supported samples.

2.6. Raman Analysis

The Raman spectra of fresh Ni-supported catalysts are shown in Figure 6. Raman signals at 414–452, 508, 582, and 611 cm⁻¹ are observed in all spectra. This is associated with the stretching of the Ni–O bond. The bulk nickel oxide shows a main signal centered at 582–611 cm⁻¹. The detected shift in the maximum frequency of this band could be related to the interaction between the alumina and nickel species [28]. Previous researchers have performed XPS analyses of NiO [29,30]. It was observed that only Ni²⁺ species were present in the Ni2p XPS spectrum, as the two peaks located at BE values of 873.1 and 871.5 eV corresponded to Ni2p1/2 of Ni(OH)₂ and NiO, respectively.

2.7. Catalyst Activity

Figure 7 exhibits the activity and stability performance in terms of the conversion and hydrogen/CO ratio of different supported Ni catalysts using CRM operated at 700 °C. The SA75 sample best converted methane and carbon dioxide, at 58.2% and 67.7%, respectively, with 0.85 H₂/CO. Conversely, the conversions of the SA39 sample displayed the lowest CH₄ and CO₂ values, of 34.7% and 31.0%, respectively, with 0.83 H₂/CO. The performance results can be related to the surface areas of supported Ni catalysts since the high-surface-area sample SA75 displayed the best performance, followed by the intermediate surface area samples of SA33 and SA35, while the low-surface-area samples SA39 and SA02 exhibited the worst performance. The overall catalytic performance of all samples was rather stable, within a reaction time of 7.5 h. The established higher conversion of CO₂ than that of CH₄ during CRM was attributed to the reverse water–gas shift reaction Equation (4) [31]. A comparison between the present work’s catalytic activity and that in the literature was performed in terms of CH₄ and CO₂ conversion under different

reaction/catalytic conditions, such as: catalyst weight, catalyst surface area, feed ratio, activation temperature, reaction temperature, and time on stream (TOS). The present catalysts displayed comparable results, as shown in Table 1.

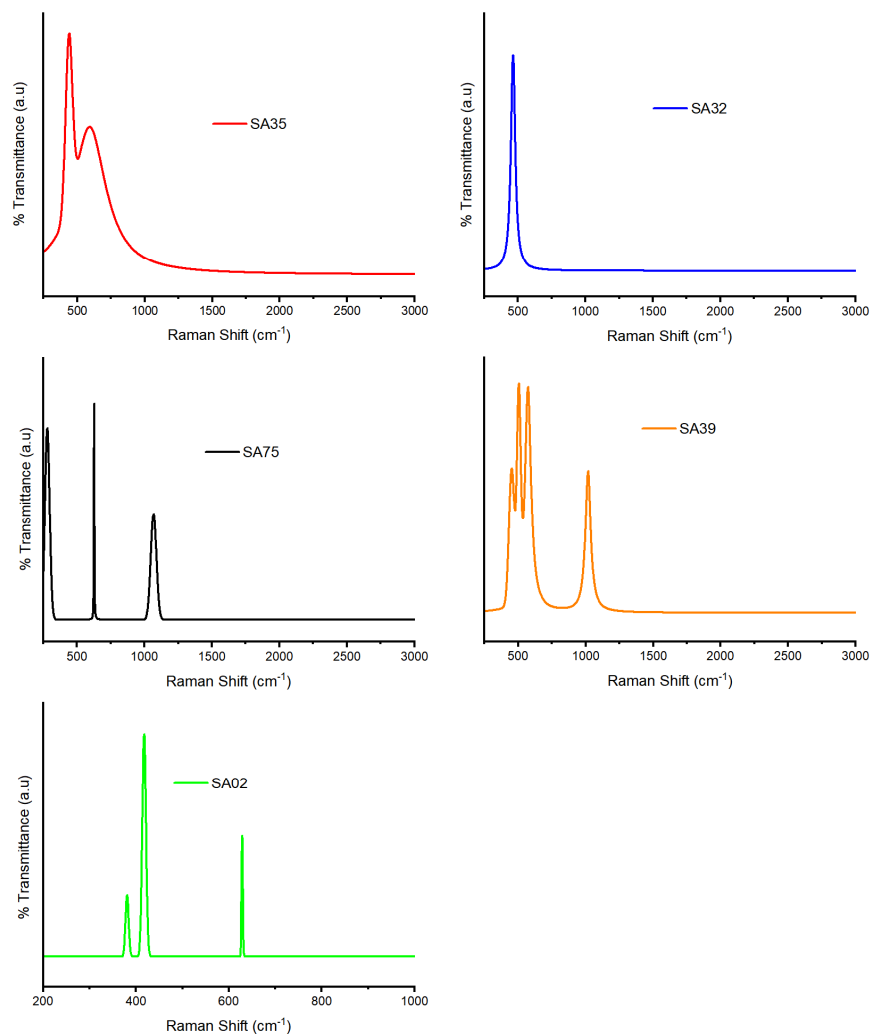


Figure 6. Fresh Raman spectra of Ni-supported samples.

Table 1. Comparison of the results of this work with those reported earlier for alumina.

Catalysts	BET (m ² /g)	Catalyst Weight (mg)	Feed Ratio			Activation Temp. (°C)	Reaction Temp. (°C)	TOS (h)	Conversion (%)		Ref.
			CO ₂	CH ₄	Inert				CH ₄	CO ₂	
5%Ni/Al ₂ O ₃	132	200	1	1	0	700	700	5	60	70	[32]
Ni/Al.550	178	-	9	9	2	700	650	8	48	52	[33]
Ni/Al	191	100	1	1	0	800	700	24	55	65	[34]
5Ni3SiAl	222.08	100	6	6	1	800	700	7	65	70	[35]
Ni/Al	189.5	300	5	5	1	600	700	6	79.9	-	[36]
5NiAl	182	100	3	3	1	600	700	7	79	85	[37]
5Ni/Al ₂ O ₃	160.8	250	3	3	14	650	650	50	57	61	[38]
Ni/γ-Al ₂ O ₃	123	-	1	1	2	700	700	20	55	64	[39]
Ni/Al ₂ O ₃	113	-	1	1	0	700	850	24	80	85	[40]
10Ni/Al ₂ O ₃	120	100	1	1	0	700	750	4	60	70	[41]
Ni/Al ₂ O ₃	200	100	1	1	0	550	450	20	8	10	[42]
SA75	260	100	3	3	1	700	700	7	58.2	67.7	This work
SA32	30	100	3	3	1	700	700	7	52.8	58.7	
SA35	12	100	3	3	1	700	700	7	43.5	50.5	
SA02	3	100	3	3	1	700	700	7	31.2	43.3	
SA39	0.3	100	3	3	1	700	700	7	24.7	31	

TOS = time on stream, Ref. = reference.

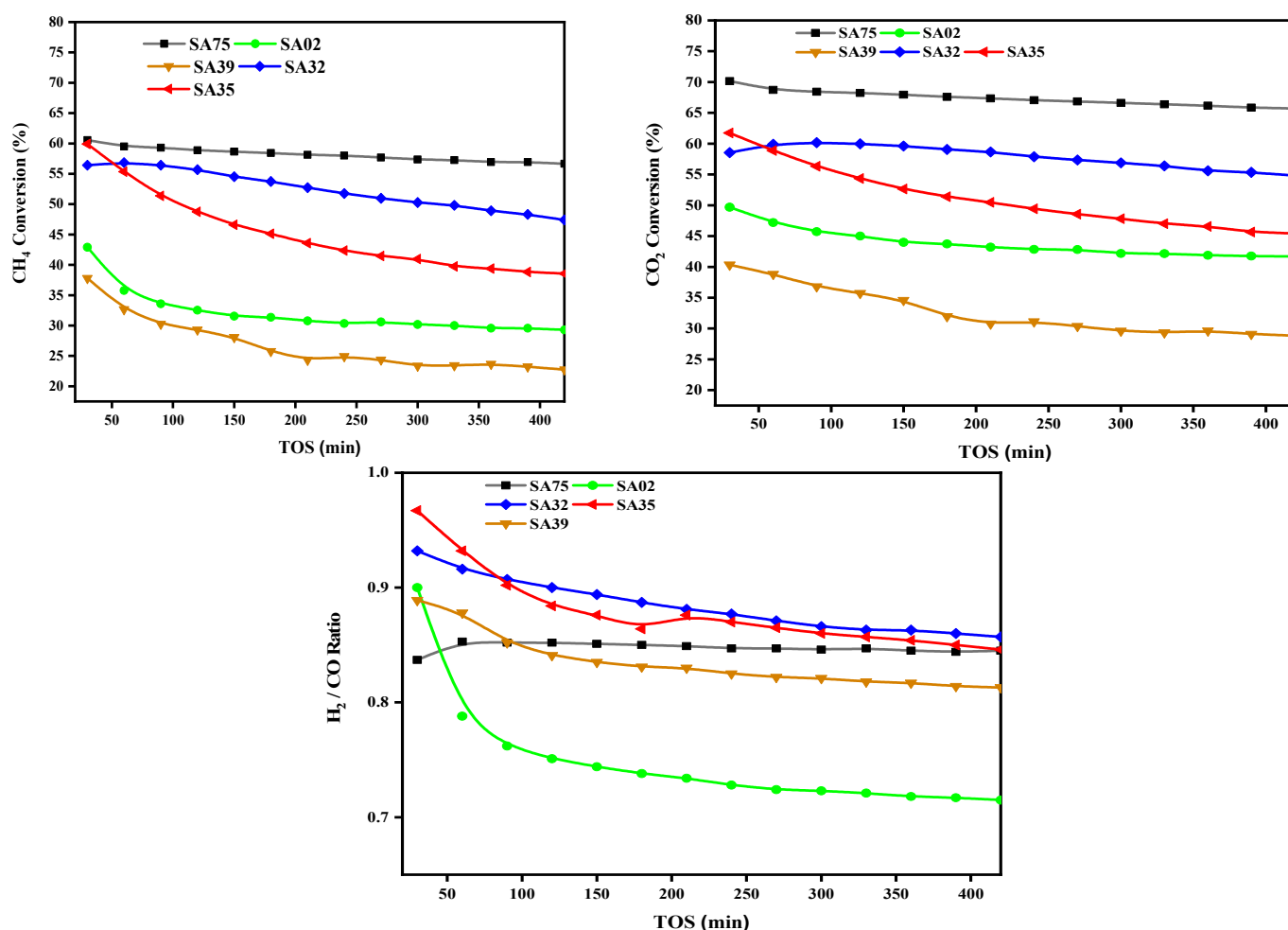


Figure 7. Conversions of CH_4 , CO_2 , and H_2/CO ratio at 700 °C, ambient pressure, and $\text{GHSV} = 48 \text{ L}/(\text{h}\cdot\text{g}_{\text{cat}})$ of the Ni-supported catalysts.

2.8. Mechanism of CRM

Figure 8 displays the summarized mechanism of CRM. The subfigures labeled with A, B, C, and D display the stages and the pathways of the mechanism. In Figure 8A, CH_4 in the feed gas is adsorbed on Ni sites of the catalyst and dissociates into CH_x and H. On the other hand, CO_2 in the feed gas is adsorbed on the metal and metal–support interface, then dissociates into O and CO. In Figure 8B, the adsorbed H on the Ni sites is combined and desorbed as H_2 , and the adsorbed CO on the support is desorbed as CO. Figure 8C demonstrates that the active sites for the large-surface-area support are sufficiently exposed in the pore and on the surface, while Figure 8D shows that the active sites are less exposed. Alternatively, Figure 8E depicts that the active sites for the low-surface-area support are least exposed in the pore and on the surface.

2.9. TGA

Figure 9 shows the results of the thermogravimetric analysis (TGA) of the used catalysts. The TGA analysis was recorded in the temperature range of 0–1000 °C during the CRM reaction for 7 h at 700 °C. The SA75 sample showed the lowest (11.2 wt.%) carbon deposition. In comparison, the samples SA39, SA02, SA32, and SA35 displayed 36.4, 28.2, 21.8, and 23.1 wt.% carbon deposition, respectively. It can be inferred that samples of low surface areas and high basicity are prone to more carbon deposition. Carbon decomposition depends on CH_4 dissociation, and the CO_2 adsorption is enhanced by the sample's basicity [43]. Here, it can also be said that sample SA75 had a good balance between acidic and basic sites, which facilitated efficient carbon removal.

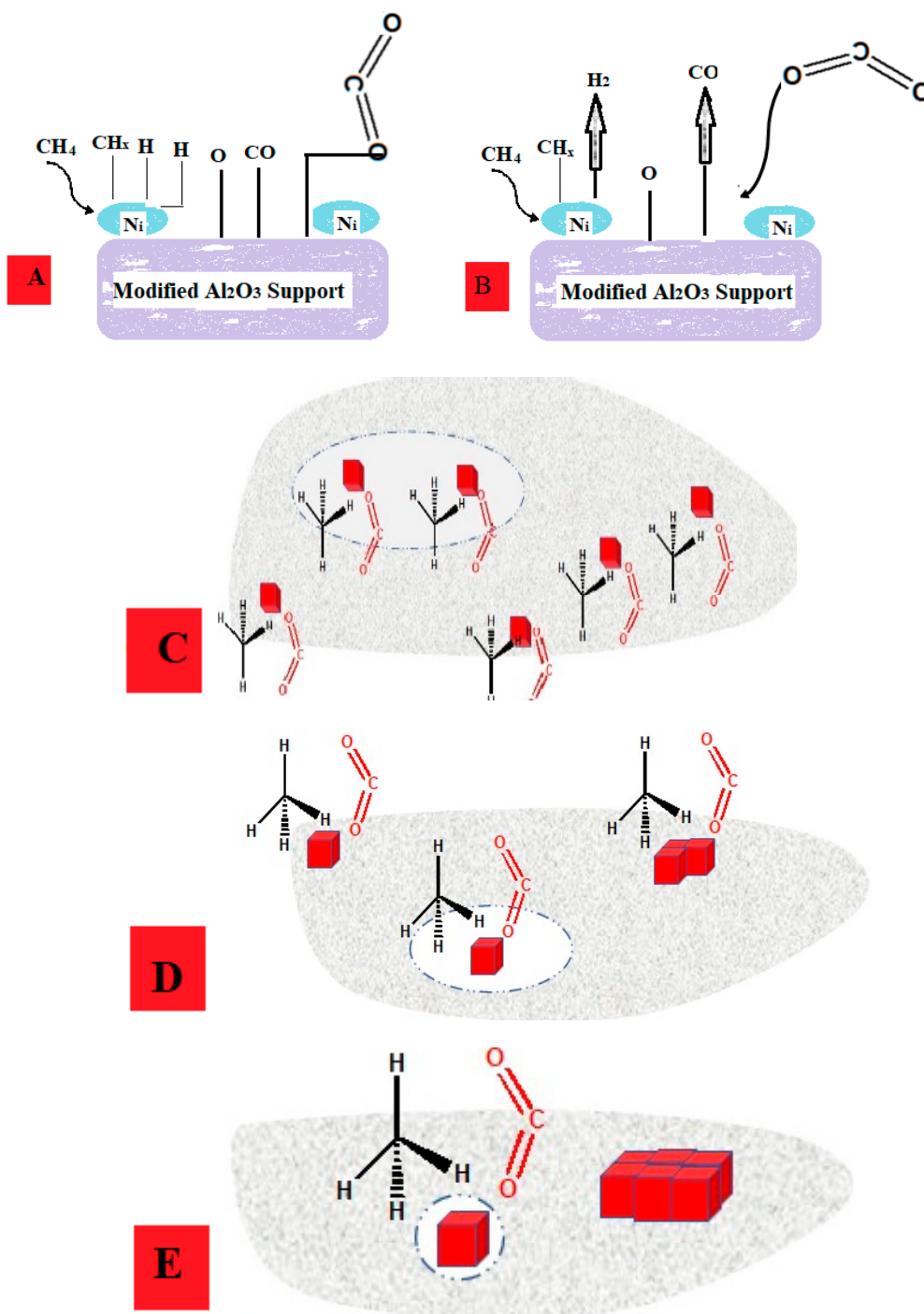


Figure 8. Reaction mechanism for the CRM process. The subfigures (A–E) display the stages and the pathways of the mechanism.

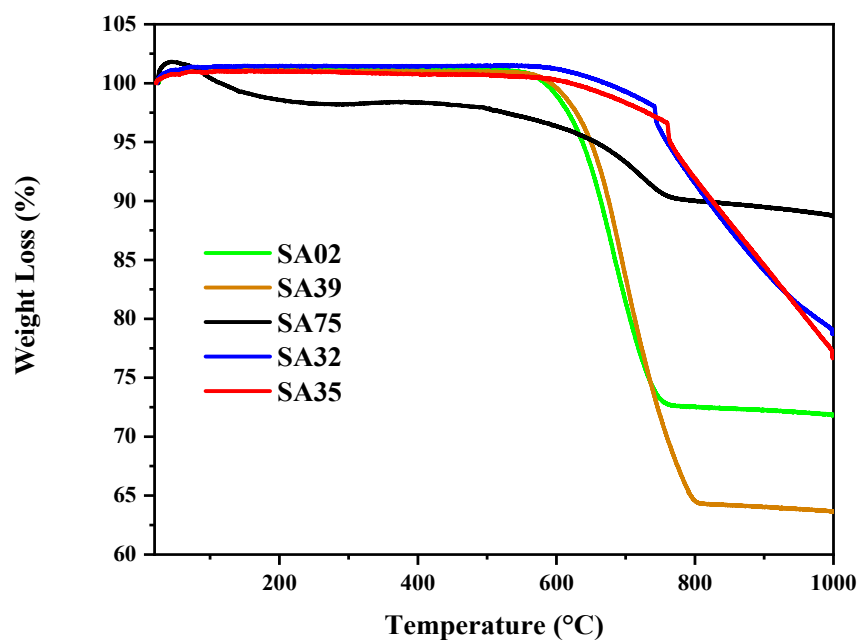


Figure 9. TGA curves for quantifying the amount of deposited carbon on the Ni-supported.

2.10. O₂-TPO

TPO is one of the beneficial techniques used in determining the type of carbon deposited onto the surface of used catalysts. The different types of carbon formed on catalyst surfaces can be gasified in different temperature ranges: <250 °C (atomic carbon), 250–600 °C (amorphous carbon), and >600 °C (graphitic carbon) [44]. Figure 10 presents the TPO profiles obtained for all catalysts after the CRM reaction for 7 h. The TPO profiles of the catalysts exhibit single broad peaks at 500–700 °C, indicating that an amorphous and graphitic blend of carbon was deposited on the catalysts. The high-surface-area sample depicts two more small peaks ascribable to atomic carbon. In general, the extent of carbon deposition is the lowest for the high-surface-area samples, followed by the intermediate-surface-area samples. Comparatively, the highest carbon formation is exhibited by the low-surface-area samples. This TPO finding is in accordance with that of the TGA profiles, with carbon deposition mainly resulting from the two reactions of Equations (5) and (6).

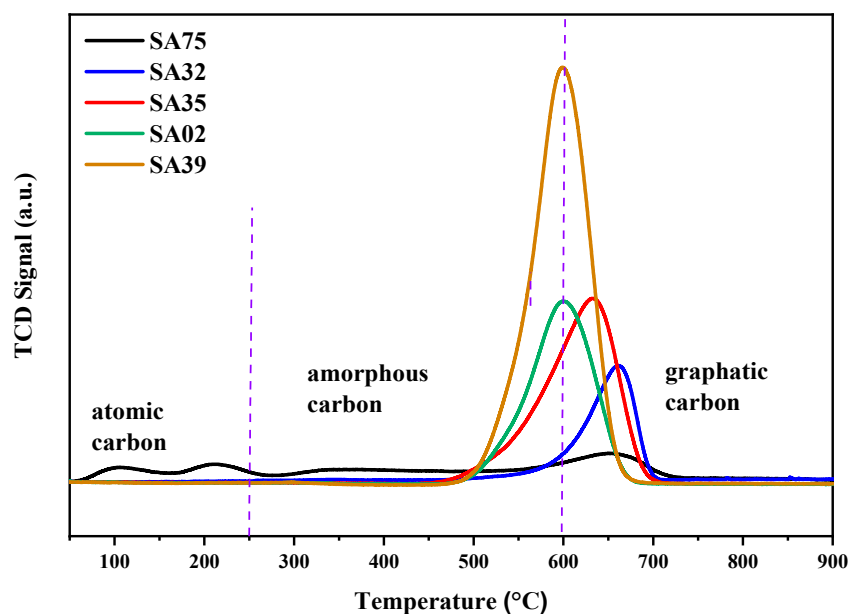


Figure 10. Temperature-programming oxidation of the used catalysts.

3. Experimental Procedure

3.1. Catalysts' Preparation

The compositions of the catalysts and the respective notations used in the text are reported in Table 1. Supports of Al₂O₃, Al₂O₃ doped with SiO₂, and nickel nitrate hexahydrate Ni (NO₃)₂·6H₂O 98%, were purchased from Alfa Aesar and used as received. Ultrapure water was obtained via a Milli-Q water purification system (Millipore). A description of the supports is provided in Table 2.

Table 2. Description of the supports used.

Support Name	Surface Area (m ² /g)	Pore Diameter	Pore Volume (cm ³ /g)	Purity (wt.%)
SA-6175	High (>120) 260.0	10 nm	0.83	<0.05% Na ₂ O
SA-3132	Intermediate (10–120) 30.0	1.2 μm	0.55	17.9% SiO ₂
SA-3135	Intermediate (10–120) 12.0	1.2 μm	0.53	17.9% SiO ₂
SA-5202	Low (0–10) 3.0	1.2 μm/ 16.1 nm	0.3/0.01	<0.05 SiO ₂
SA-5239	Low (0–10) 0.3	1.8/150 μm	0.43	12% SiO ₂

3.2. Synthesis of Catalysts

A two-step synthesis procedure, based on the incipient wetness impregnation method, was utilized for the preparation of all catalysts. The first step was the synthesis of the alumina support or alumina doped with SiO₂. The second step was loading the active catalyst, nickel oxide with 5.0 wt.%, on the various supports. Al₂O₃ and the alumina doped with SiO₂-supported Ni-based catalysts were prepared by the incipient impregnation method with a Ni loading of 5%. An aqueous solution containing the desired amount of Ni (NO₃)₂·6H₂O was added to the support and then dried slowly in a rotary evaporator under a vacuum at 80 °C for 2 h, followed by drying at 120 °C in an oven overnight and calcining in the air at 700 °C for 3 h. The 5% Ni supported on SA-6175, SA-3132, SA-3135, SA-5202, and SA-5239 catalysts are referred to as: SA75, SA32, SA35, SA02, and SA39, respectively. Table 3 gives descriptions of the prepared catalysts.

Table 3. Description of the used catalysts.

Catalyst Tested	Catalyst's Abbreviated Name	Surface Area (m ² /g)	Pore Volume (cm ³ /g)	Pore Size (nm)
5% Ni/SA-6175	SA75	189.0	0.66	12.8
5% Ni/SA-3132	SA32	25.3	0.14	22.5
5% Ni/SA-3135	SA35	15.6	0.11	30.0
5% Ni/SA-5202	SA02	2.7	0.01	17.4
5% Ni/SA-5239	SA39	2.3	0.01	17.0

3.3. Catalyst Characterization

The Ni-supported catalysts' surface area, and the pore size and pore diameter, were determined by N₂ adsorption–desorption at −196 °C using a Micromeritics Tristar II 3020 for porosity and a surface area analyzer. Temperature-programming processes comprising H₂-TPR, CO₂-TPD, and O₂-TPO were performed on a Micromeritics Auto Chem II 2920. The tests were done over a temperature range of 50–900 °C with a 2.40 L/h flow of 10% H₂/Ar mixture for the H₂-TPR analysis, 10% CO₂/He mixture for the CO₂-TPD basicity measurement, and 10% O₂/He mixture for the O₂-TPO carbon-type assessment. The X-ray

diffraction patterns of the catalysts were registered on a Miniflex Rigaku diffractometer equipped with Cu K α X-ray radiation. The device was run at 40 kV and 40 mA. The extent of carbon deposition on the used catalysts was measured by thermo-gravimetric (TGA) analysis. Here, a platinum pan was filled with 10–15 mg of the spent catalysts. It was heated at 25 °C up to 1000 °C at a 20 °C min⁻¹ temperature ramp. Mass variations were continuously monitored as the heating progressed. Fourier transform infrared spectroscopy (FTIR) using IR Prestige-21 SHMADZU was used to study the surface properties and functional groups in the samples.

3.4. Catalytic Activity Test

The catalysts were tested for CRM at a 700 °C reaction temperature under atmospheric pressure. A packed bed stainless steel reactor (internal diameter: 9.1 mm; height: 300 mm) was used to perform the experiments. A catalyst mass of 0.10 g was positioned in the reactor over a ball of glass wool. A stainless-steel sheathed thermocouple, K-type, axially positioned close to the catalyst bed was used to read the temperature during the reaction. Prior to the reaction, activation of the catalysts was performed at 700 °C in an atmosphere of H₂. This lasted for an hour and the remnant H₂ was purged with N₂. During the CRM reaction, the feed volume ratio was kept at 3:3:1 for CH₄, CO₂, and N₂ gases, respectively, with a space velocity of 42 L/h./g_{cat}. The outlet gas from the reactor was connected to online gas chromatography (GC) with a thermal conductivity detector to compute its composition. The CH₄ and CO₂ conversions and the syngas ratio were calculated as follows:

$$\text{CH}_4 \text{ Conversion (\%)} = \frac{(\text{CH}_4)_{\text{in}} - (\text{CH}_4)_{\text{out}}}{(\text{CH}_4)_{\text{in}}} \times 100 \quad (7)$$

$$\text{CO}_2 \text{ Conversion (\%)} = \frac{(\text{CO}_2)_{\text{in}} - (\text{CO}_2)_{\text{out}}}{(\text{CO}_2)_{\text{in}}} \times 100 \quad (8)$$

$$\frac{\text{H}_2}{\text{CO}} = \frac{\text{generated moles of H}_2}{\text{generated moles of CO}} \quad (9)$$

4. Conclusions

The different Ni-supported catalyst samples used for CRM at 700 °C showed variation in their activity and stability performances. The SA75 sample displayed the highest methane and carbon dioxide conversions, with a H₂/CO ratio close to unity. Alternatively, the SA39 sample provided the lowest conversions of CH₄ and CO₂. The TPR analysis revealed that the low-surface-area samples SA39 and SA02 exhibited moderate interactions between NiO and the support, whilst the high-surface-area sample SA75 showed powerful interactions between Ni and the support. The XRD profiles exhibited by the crystals of NiO, Al₂O₃, and SiO₂ and the spinel compound between Ni and the alumina support were ascertained. Analysis of the CO₂-TPD of the low-surface-area samples SA39 and SA02 revealed the availability of strong basic sites, which took part in the efficiency decline. In the TGA analysis, the high-surface-area sample SA75 showed the least carbon deposition. The TPO profiles of the catalysts exhibited single broad peaks at 500–700 °C, indicating that an amorphous and graphitic blend of carbon was deposited on the catalysts. Good correspondence was attained between the TGA and TPO profiles.

Author Contributions: Methodology and supervision of preparation of catalysts, S.B.A. and A.M.A.; formal analysis, writing—original draft preparation, and preparation of catalysts, A.A.I. and A.S.A.-F.; project administration, funding acquisition, and writing—review and editing, A.H.F. and F.A.A.A. All authors have read and agreed to the published version of the manuscript.

Funding: The authors would like to sincerely thank the Researchers Supporting Project (number RSP-2021/368), King Saud University, Riyadh, Saudi Arabia.

Data Availability Statement: Not applicable.

Acknowledgments: The KSU authors would like to extend their sincere appreciation to the Researchers Supporting Project (number RSP-2021/368), King Saud University, Riyadh, Saudi Arabia.

Conflicts of Interest: The authors declare an absence of conflict of interest.

References

1. Akri, M.; Zhao, S.; Li, X.; Zang, K.; Lee, A.F.; Isaacs, M.A.; Xi, W.; Gangarajula, Y.; Luo, J.; Ren, Y.; et al. Atomically dispersed nickel as coke-resistant active sites for methane dry reforming. *Nat. Commun.* **2019**, *10*, 5181–5191. [[CrossRef](#)] [[PubMed](#)]
2. Azevedo, I.R.; da Silva, A.A.A.; Xing, Y.T.; Rabelo-Neto, R.C.; Luchters, N.T.J.; Fletcher, J.C.Q.; Noronha, F.B.; Mattos, L.V. Long-term stability of Pt/Ce_{0.8}Me_{0.2}O₂- γ /Al₂O₃ (Me=Gd, Nb, Pr, and Zr) catalysts for steam reforming of methane. *Int. J. Hydrogen Energy* **2022**, *47*, 15624–15640. [[CrossRef](#)]
3. Araújo, J.C.S.; Oton, L.F.; Bessa, B.; Neto, A.B.S.; Oliveira, A.C.; Lang, R.; Otubo, L.; Bueno, J.M.C. The role of Pt loading on La₂O₃-Al₂O₃ support for methane conversion reactions via partial oxidation and steam reforming. *Fuel* **2019**, *254*, 115681–115696. [[CrossRef](#)]
4. Ruan, G.; Zhang, Z.; Metals, M.Y.-R. Undefined Effect of SiO₂ micro powder on properties of corundum-mullite composites. *Rare Met.* **2011**, *30*, 506–510. [[CrossRef](#)]
5. Therdthianwong, S.; Siangchin, C.; Therdthianwong, A. Improvement of coke resistance of Ni/Al₂O₃ catalyst in CH₄/CO₂ reforming by ZrO₂ addition. *Fuel Process. Technol.* **2008**, *89*, 160–168. [[CrossRef](#)]
6. Pompeo, F.; Nichio, N.N.; Souza, M.M.V.M.; Cesar, D.V.; Ferretti, O.A.; Schmal, M. Study of Ni and Pt catalysts supported on α -Al₂O₃ and ZrO₂ applied in methane reforming with CO₂. *Appl. Catal. A Gen.* **2007**, *316*, 175–183. [[CrossRef](#)]
7. Moogi, S.; Hyun Ko, C.; Hoon Rhee, G.; Jeon, B.H.; Ali Khan, M.; Park, Y.K. Influence of catalyst synthesis methods on anti-coking strength of perovskites derived catalysts in biogas dry reforming for syngas production. *Chem. Eng. J.* **2022**, *437*, 135348. [[CrossRef](#)]
8. Da Costa-Serra, J.F.; Chica, A. Bioethanol steam reforming on Co/ITQ-18 catalyst: Effect of the crystalline structure of the delaminated zeolite ITQ-18. *Int. J. Hydrogen Energy* **2011**, *36*, 3862–3869. [[CrossRef](#)]
9. Da Costa-Serra, J.F.; Guil-López, R.; Chica, A. Co/ZnO and Ni/ZnO catalysts for hydrogen production by bioethanol steam reforming. Influence of ZnO support morphology on the catalytic properties of Co and Ni active phases. *Int. J. Hydrogen Energy* **2010**, *35*, 6709–6716. [[CrossRef](#)]
10. Zhou, L.; Li, L.; Wei, N.; Li, J.; Basset, J.M. Effect of NiAl₂O₄ Formation on Ni/Al₂O₃ Stability during Dry Reforming of Methane. *ChemCatChem* **2015**, *7*, 2508–2516. [[CrossRef](#)]
11. Zhang, L.; Zhang, Q.; Liu, Y.; Zhang, Y. Dry reforming of methane over Ni/MgO-Al₂O₃ catalysts prepared by two-step hydrothermal method. *Appl. Surf. Sci.* **2016**, *389*, 25–33. [[CrossRef](#)]
12. Fuentes, A.; Da Costa-Serra, J.F.; Chica, A. New Catalysts based on Ni-Birnessite and Ni-Todorokite for the Efficient Production of Hydrogen by Bioethanol Steam Reforming. *Energy Procedia* **2012**, *29*, 181–191. [[CrossRef](#)]
13. Wang, F.; Xu, L.; Zhang, J.; Zhao, Y.; Li, H.; Li, H.X.; Wu, K.; Xu, G.Q.; Chen, W. Tuning the metal-support interaction in catalysts for highly efficient methane dry reforming reaction. *Appl. Catal. B Environ.* **2016**, *180*, 511–520. [[CrossRef](#)]
14. Elharati, M.A.; Lee, K.M.; Hwang, S.; Mohammed Hussain, A.; Miura, Y.; Dong, S.; Fukuyama, Y.; Dale, N.; Saunders, S.; Kim, T.; et al. The effect of silica oxide support on the catalytic activity of nickel-molybdenum bimetallic catalyst toward ethanol steam reforming for hydrogen production. *Chem. Eng. J.* **2022**, *441*, 135916. [[CrossRef](#)]
15. Xu, Y.; Du, X.H.; Li, J.; Wang, P.; Zhu, J.; Ge, F.J.; Zhou, J.; Song, M.; Zhu, W.Y. A comparison of Al₂O₃ and SiO₂ supported Ni-based catalysts in their performance for the dry reforming of methane. *J. Fuel Chem. Technol.* **2019**, *47*, 199–208. [[CrossRef](#)]
16. Zhang, Y.; Zeng, R.; Zu, Y.; Zhu, L.; Mei, Y.; Luo, Y.; He, D. Low-temperature dry reforming of methane tuned by chemical speciations of active sites on the SiO₂ and γ -Al₂O₃ supported Ni and Ni-Ce catalysts. *Chin. J. Chem. Eng.* **2022**, *48*, 76–90. [[CrossRef](#)]
17. Rabelo-Neto, R.C.; Sales, H.B.E.; Inocência, C.V.M.; Varga, E.; Oszko, A.; Erdohelyi, A.; Noronha, F.B.; Mattos, L.V. CO₂ reforming of methane over supported LaNiO₃ perovskite-type oxides. *Appl. Catal. B Environ.* **2018**, *221*, 349–361. [[CrossRef](#)]
18. Cao, P.; Zhao, H.; Adegbite, S.; Yang, B.; Lester, E.; Wu, T. Stabilized CO₂ reforming of CH₄ on modified Ni/Al₂O₃ catalysts via in-situ K₂CO₃-enabled dynamic coke elimination reaction. *Fuel* **2021**, *298*, 120599. [[CrossRef](#)]
19. Garbarino, G.; Phung, T.K.; Pampararo, G.; Riani, P.; Busca, G. Modification of the properties of γ -alumina as a support for nickel and molybdate catalysts by addition of silica. *Catal. Today* **2021**, *378*, 57–64. [[CrossRef](#)]
20. Maryam, K.M.; Huang, B.; Calvin, H.B.; Todd, M.A.; Brian, F.W. Synthesis and characterization of silica doped alumina catalyst support with superior thermal stability and unique pore properties. *J. Porous Mater.* **2016**, *23*, 475–487. [[CrossRef](#)]
21. Thommes, M.; Kaneko, K.; Neimark, A.V.; Olivier, J.P.; Rodriguez-Reinoso, F.; Rouquerol, J.; Sing, K.S.W. Physisorption of gases, with special reference to the evaluation of surface area and pore size distribution (IUPAC Technical Report). *Pure Appl. Chem.* **2015**, *87*, 1051–1069. [[CrossRef](#)]
22. Xu, X.; Wang, Y.; Hao, M.; Bai, J.; Fang, B.; Liang, J.; Gao, P.; Ding, Y.; Li, H.; Wang, F. A simple fabrication of mineral supported Ni-NiAl₂O₄ nanocomposites with a novel transition layer. *Mater. Charact.* **2022**, *192*, 112194. [[CrossRef](#)]
23. Pettit, F.S.; Randklev, E.H.; Felten, E.J. Formation of NiAl₂O₄ by Solid State Reaction. *J. Am. Ceram. Soc.* **1966**, *49*, 199–203. [[CrossRef](#)]

24. Yang, R.; Qi, Z.; Gao, Y.; Yang, J.; Zhou, Y.; Liu, H.; Peng, L.; Jiao, J. Effects of alumina sols on the sintering of α -alumina ceramics. *Ceram. Int.* **2020**, *46*, 20865–20870. [[CrossRef](#)]
25. Vlaev, L.; Damyanov, D.; Mohamed, M.M. Infrared spectroscopy study of the nature and reactivity of a hydrate coverage on the surface of γ -Al₂O₃. *Colloids Surf.* **1989**, *36*, 427–437. [[CrossRef](#)]
26. Calatayud, M.; Collins, S.E.; Baltanás, M.A.; Bonivardi, A.L. Stability of formate species on β -Ga₂O₃. *Phys. Chem. Chem. Phys.* **2009**, *11*, 1397–1405. [[CrossRef](#)] [[PubMed](#)]
27. Reshetenko, T.V.; Avdeeva, L.B.; Khassin, A.A.; Kustova, G.N.; Ushakov, V.A.; Moroz, E.M.; Shmakov, A.N.; Kriventsov, V.V.; Kochubey, D.I.; Pavlyukhin, Y.T.; et al. Coprecipitated iron-containing catalysts (Fe-Al₂O₃, Fe-Co-Al₂O₃, Fe-Ni-Al₂O₃) for methane decomposition at moderate temperatures I. Genesis of calcined and reduced catalysts. *Appl. Catal. A Gen.* **2004**, *268*, 127–138. [[CrossRef](#)]
28. Ghule, A.V.; Ghule, K.; Punde, T.; Liu, J.Y.; Tzing, S.H.; Chang, J.Y.; Chang, H.; Ling, Y.C. In situ monitoring of NiO–Al₂O₃ nanoparticles synthesis by thermo-Raman spectroscopy. *Mater. Chem. Phys.* **2010**, *119*, 86–92. [[CrossRef](#)]
29. Shi, Y.; Tian, S.; Shi, Q.; Zhang, Y.; Waheed, A.; Cao, Y.; Li, G. Cascade Aldol Condensation of an Aldehyde via the Aerobic Oxidation of Ethanol over an Au/NiO Composite. *Nanoscale Adv.* **2019**, *1*, 3654–3659. [[CrossRef](#)]
30. Cao, Y.; Su, Y.; Xu, L.; Yang, X.; Han, Z.; Cao, R.; Li, G. Ionic liquids modified oxygen vacancy-rich amorphous FeNi hydroxide nanoclusters on carbon-based materials as an efficient electrocatalyst for electrochemical water oxidation. *J. Energy Chem.* **2022**, *71*, 167–173. [[CrossRef](#)]
31. Gunduz-Meric, G.; Kaytakoglu, S.; Degirmenci, L. Ni,Co/SiO₂ and Ni/SiO₂,Co bimetallic microsphere catalysts indicating high activity and stability in the dry reforming of methane. *React. Kinet. Mech. Catal.* **2020**, *129*, 403–419. [[CrossRef](#)]
32. Deb, M.; Banerjee, R.; Majumder, A.; Sastry, G.R.K. Multi objective optimization of performance parameters of a single cylinder diesel engine with hydrogen as a dual fuel using pareto-based genetic algorithm. *Int. J. Hydrogen Energy* **2014**, *39*, 8063–8077. [[CrossRef](#)]
33. Ha, Q.L.M.; Armbruster, U.; Atia, H.; Schneider, M.; Lund, H.; Agostini, G.; Radnik, J.; Vuong, H.T.; Martin, A. Development of Active and Stable Low Nickel Content Catalysts for Dry Reforming of Methane. *Catalysts* **2017**, *7*, 157. [[CrossRef](#)]
34. Fouskas, A.; Kollia, M.; Kambolis, A.; Papadopoulou, C.; Matralis, H. Boron-modified Ni/Al₂O₃ catalysts for reduced carbon deposition during dry reforming of methane. *Appl. Catal. A Gen.* **2014**, *474*, 125–134. [[CrossRef](#)]
35. Al-Fatesh, A.S.; Kumar, R.; Kasim, S.O.; Ibrahim, A.A.; Fakeeha, A.H.; Abasaeed, A.E.; Alrasheed, R.; Bagabas, A.; Chaudhary, M.L.; Frusteri, F.; et al. The effect of modifier identity on the performance of Ni-based catalyst supported on γ -Al₂O₃ in dry reforming of methane. *Catal. Today* **2020**, *348*, 236–242. [[CrossRef](#)]
36. Al-Fatesh, A.S.; Naeem, M.A.; Fakeeha, A.H.; Abasaeed, A.E. CO₂ Reforming of Methane to Produce Syngas over γ -Al₂O₃-Supported Ni–Sr Catalysts. *Bull. Chem. Soc. Jpn.* **2013**, *86*, 742–748. [[CrossRef](#)]
37. Fakeeha, A.H.; Bagabas, A.A.; Lanre, M.S.; Osman, A.I.; Kasim, S.O.; Ibrahim, A.A.; Arasheed, R.; Alkhalifa, A.; Elnour, A.Y.; Abasaeed, A.E.; et al. Catalytic Performance of Metal Oxides Promoted Nickel Catalysts Supported on Mesoporous γ -Alumina in Dry Reforming of Methane. *Process* **2020**, *8*, 522. [[CrossRef](#)]
38. Li, K.; Pei, C.; Li, X.; Chen, S.; Zhang, X.; Liu, R.; Gong, J. Dry reforming of methane over La₂O₂CO₃-modified Ni/Al₂O₃ catalysts with moderate metal support interaction. *Appl. Catal. B Environ.* **2020**, *264*, 118448. [[CrossRef](#)]
39. Amin, M.H.; Mantri, K.; Newnham, J.; Tardio, J.; Bhargava, S.K. Highly stable ytterbium promoted Ni/ γ -Al₂O₃ catalysts for carbon dioxide reforming of methane. *Appl. Catal. B Environ.* **2012**, *119*, 217–226. [[CrossRef](#)]
40. Rahemi, N.; Haghghi, M.; Babaluo, A.A.; Jafari, M.F.; Khorram, S. Non-thermal plasma assisted synthesis and physicochemical characterizations of Co and Cu doped Ni/Al₂O₃ nanocatalysts used for dry reforming of methane. *Int. J. Hydrogen Energy* **2013**, *38*, 16048–16061. [[CrossRef](#)]
41. Chein, R.Y.; Fung, W.Y. Syngas production via dry reforming of methane over CeO₂ modified Ni/Al₂O₃ catalysts. *Int. J. Hydrogen Energy* **2019**, *44*, 14303–14315. [[CrossRef](#)]
42. Song, Z.; Wang, Q.; Guo, C.; Li, S.; Yan, W.; Jiao, W.; Qiu, L.; Yan, X.; Li, R. Improved effect of Fe on the stable NiFe/Al₂O₃ catalyst in low-temperature dry reforming of methane. *Ind. Eng. Chem. Res.* **2020**, *59*, 17250–17258. [[CrossRef](#)]
43. Zhang, S.; Shi, C.; Chen, B.; Zhang, Y.; Qiu, J. An active and coke-resistant dry reforming catalyst comprising nickel-tungsten alloy nanoparticles. *Catal. Commun.* **2015**, *69*, 123–128. [[CrossRef](#)]
44. Shen, J.; Reule, A.A.C.; Semagina, N. Ni/MgAl₂O₄ catalyst for low-temperature oxidative dry methane reforming with CO₂. *Int. J. Hydrogen Energy* **2019**, *44*, 4616–4629. [[CrossRef](#)]